

The Orientation Dependence of Cavity-Modified Chemistry

Marcus Dante Liebenthal and A. Eugene DePrince III^{a)}

Department of Chemistry and Biochemistry, Florida State University, Tallahassee, FL 32306-4390

Recent theoretical studies have explored how ultra-strong light–matter coupling can be used as a handle to control chemical transformations. *Ab initio* cavity quantum electrodynamics (QED) calculations demonstrate that large changes to reaction energies or barrier heights can be realized by coupling electronic degrees of freedom to vacuum fluctuations associated with an optical cavity mode, provided that large enough coupling strengths can be achieved. In many cases, the cavity effects display a pronounced orientational dependence. In this Perspective, we highlight the critical role that geometry relaxation can play in such studies. As an example, we consider recent work [Nat. Commun. **14**, 2766 (2023)] that explored the influence of an optical cavity on Diels-Alder cycloaddition reactions and reported large changes to reaction enthalpies and barrier heights, as well as the observation that changes in orientation can inhibit the reaction or select for one reaction product or another. Those calculations used fixed molecular geometries optimized in the absence of the cavity and fixed relative orientations of the molecules and the cavity mode polarization axis. Here, we show that, when given a chance to relax in the presence of the cavity, the molecular species reorient in a way that eliminates the orientational dependence. Moreover, in this case, we find that qualitatively different conclusions regarding the impact of the cavity on the thermodynamics of the reaction can be drawn from calculations that consider relaxed versus unrelaxed molecular structures.

I. INTRODUCTION

Strong interactions between light and matter can induce nontrivial changes in molecular properties and chemical reactivity. Such interactions have been leveraged experimentally as a means of augmenting material properties^{1–5} and controlling chemical transformations carried out within optical cavities.^{6–11} Given these exciting prospects, substantial computational and theoretical effort has been undertaken to develop both effective theories¹² for simulating collective strong coupling effects and quantum electrodynamics generalizations of familiar *ab initio* quantum chemistry methods¹³ for modeling cavity-induced changes to electronic structure in the single-molecule strong coupling limit. In the latter category, the last decade has seen the development and application of QED generalizations of many quantum chemistry methods, including density functional theory (QEDFT^{14–23} or QED-DFT^{24–28}) configuration interaction (QED-CI),^{29–32} coupled-cluster theory (QED-CC),^{25,26,29,33–46} and more.^{47–49}

Many *ab initio* QED studies have focused on ground-state effects, exploring how vacuum fluctuations modify ground-state electronic structure and how these changes can be leveraged for useful purposes in chemistry applications. Within these studies, a common theme emerges: ground-state cavity effects have a pronounced orientational dependence. Specific examples using various *ab initio* QED approaches include the following. Vu, McLeod, Hanson, and DePrince²⁴ applied time-dependent QED-DFT to model cavity-embedded BINOL ([1,1'-binaphthalene]-2,2'-diol) derivatives in the context of the enantiopurification of BINOL via chiral-group directed photoisomerization.⁵⁰ This work found that the diastereometric excess predicted in the absence of the cavity could be enhanced, suppressed, or even inverted, depending on the relative orientation of the molecule and the cavity-mode polarization axis. Pavošević, Hammes-Schiffer, Rubio,

and Flick³⁹ used QED-CC to study cavity effects on proton transfer reactions in malonaldehyde and aminopropenal. This work found that the reaction barrier height can increase or decrease depending on the molecule's orientation in the cavity. Pavošević, Smith, and Rubio demonstrated using QED-CC that similar enhancement / inhibition could be achieved in Diels-Alder reactions of cyclopentadiene and acrylonitrile⁴² and azide-alkyne cycloaddition reactions.⁴³ These studies also showed that orientational control could be used to selectively steer the system toward a specific reaction product. Severi and Zerbetto⁵¹ used a QED generalization of Hartree-Fock theory to show that the barrier to isomerization in butadiene can be enhanced or suppressed depending on the relative orientations of the molecule and cavity mode polarization axis. Haugland, Schäfer, Ronca, Rubio, and Koch²⁹ have also shown using QED-CC and QED full CI that intermolecular interactions can be modulated in a way that stabilizes or destabilizes non-covalently bound complexes, depending on how they are oriented in the cavity.

These studies all suggest that subtle quantum electrodynamical effects can be used to dictate chemical outcomes, assuming sufficiently strong electron-photon coupling can be achieved. Equally exciting is the level of control over selectivity, etc., that these studies imply can be achieved, given absolute control over molecular orientation. For gas or solution-phase reactions, however, such control is not necessarily possible, and, yet, essentially all *ab initio* QED studies assume (i) fixed orientations relative to the cavity mode polarization axis and (ii) fixed molecular geometries that are not optimized to account for any cavity interactions. Relatively little effort has gone into understanding how molecular geometries can be perturbed by cavity forces and whether claims of orientation-based selectivity are robust to such geometry relaxation effects. As a result, the literature may overstate the prospects cavity-based control over ground-state chemistry arising from electronic strong coupling.

In this work, we consider the importance of cavity-induced geometry relaxation effects in computational studies of cavity-modified chemistry. As a model system, we choose

^{a)}Electronic mail: adeprince@fsu.edu

to revisit the Diels-Alder cycloaddition of cavity-embedded cyclopentadiene and acrylonitrile that was studied by Pavošević, Smith, and Rubio in Ref. 42 (see Fig. 1). We develop analytic energy gradients for the QED-DFT approach, which we use to optimize structures of the relevant cavity-embedded species in order to provide a side-by-side comparison of thermodynamic properties inferred from unperturbed geometries and perturbed geometries obtained at various initial relative orientations of the molecular species and cavity mode polarization axis. In short, without some physical mechanism to fix the molecular orientation, the system will reorient in a way that eliminates the orientational dependence of the reaction barrier heights and enthalpies for this cycloaddition reaction.

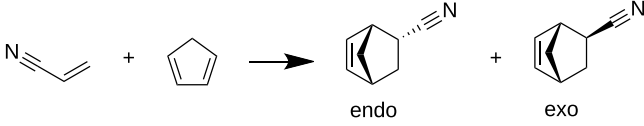


FIG. 1. The Diels-Alder cycloaddition of cyclopentadiene and acrylonitrile, forming either the *endo* or *exo* diastereomer.

II. THEORY

The physics of a strongly-coupled light-matter system is captured by the Pauli-Fierz (PF) Hamiltonian,^{52,53} which can be derived from a minimal coupling or “p · A” Hamiltonian.⁵⁴ The PF Hamiltonian is obtained via a transformation of the p · A Hamiltonian to the length gauge (*i.e.*, using the Power-Zienau-Woole transformation), followed by a phase transformation and the use of the dipole approximation. Following some straightforward but tedious manipulations, one eventually arrives at

$$\begin{aligned} \hat{H}_{\text{PF}} = & \hat{H}_e + \omega_{\text{cav}} \hat{b}^\dagger \hat{b} - \sqrt{\frac{\omega_{\text{cav}}}{2}} \boldsymbol{\lambda} \cdot \hat{\boldsymbol{\mu}} (\hat{b}^\dagger + \hat{b}) \\ & + \frac{1}{2} (\boldsymbol{\lambda} \cdot \hat{\boldsymbol{\mu}})^2 \end{aligned} \quad (1)$$

Here, the first two terms (\hat{H}_e and $\omega_{\text{cav}} \hat{b}^\dagger \hat{b}$) represent the electronic and photon Hamiltonians, respectively, and ω_{cav} is the cavity mode frequency. The symbols \hat{b}^\dagger and \hat{b} represent photon creation and annihilation operators, respectively. The third and fourth terms are the bilinear coupling and dipole self-energy terms, respectively. In these terms, we find the molecular dipole operator, $\hat{\boldsymbol{\mu}}$, and the coupling strength vector, $\boldsymbol{\lambda}$, which is related to the effective cavity mode volume (V_{eff}) and is oriented along the transverse polarization vector, \hat{e} :

$$\boldsymbol{\lambda} = \lambda \hat{e} = \sqrt{\frac{4\pi}{V_{\text{eff}}}} \hat{e} \quad (2)$$

The Hamiltonian in Eq. 1 describes coupling between electronic degrees of freedom and a single cavity mode, but it can easily be generalized to account for multiple modes.

A. QED-DFT Ground-State Energy

To model the ground-state of \hat{H}_{PF} , we use a quantum-electrodynamics generalization of density functional theory (DFT) that resembles conventional Kohn-Sham DFT,⁵⁵ augmented by a mean-field description of electron-photon interactions. We begin by considering a mean-field solution to the entire polaritonic problem (*i.e.*, QED Hartree-Fock, or QED-HF), in which case the wave function for the system has the form

$$|\Phi_0\rangle = |0^e\rangle \otimes |0^p\rangle \quad (3)$$

Here, $|0^e\rangle$ is a Slater determinant of electronic orbitals and $|0^p\rangle$ is a zero-photon state. As described in Ref. 33, it is convenient to define the photon part of $|\Phi_0\rangle$ as

$$|0^p\rangle = \hat{U}_{\text{CS}} |0\rangle \quad (4)$$

where $|0\rangle$ is the photon vacuum state, and \hat{U}_{CS} is a unitary coherent-state transformation operator

$$\hat{U}_{\text{CS}} = \exp(z(\hat{b}^\dagger - \hat{b})) \quad (5)$$

with

$$z = \frac{-\boldsymbol{\lambda} \cdot \langle \hat{\boldsymbol{\mu}} \rangle}{\sqrt{2\omega_{\text{cav}}}} \quad (6)$$

The expectation value of \hat{H}_{PF} with respect to $|\Phi_0\rangle$ is

$$\begin{aligned} E_{\text{QED-HF}} = \langle \Phi_0 | \hat{H}_{\text{PF}} | \Phi_0 \rangle &= \langle 0^e | \otimes \langle 0^p | \hat{H}_{\text{PF}} | 0^p \rangle \otimes | 0^e \rangle \\ &= \langle 0^e | \otimes \langle 0 | \hat{U}_{\text{CS}}^\dagger \hat{H}_{\text{PF}} \hat{U}_{\text{CS}} | 0 \rangle \otimes | 0^e \rangle \\ &= \langle 0^e | \otimes \langle 0 | \hat{H}_{\text{CS}} | 0 \rangle \otimes | 0^e \rangle \end{aligned} \quad (7)$$

where the coherent-state transformed Hamiltonian, \hat{H}_{CS} , is

$$\begin{aligned} \hat{H}_{\text{CS}} = & \hat{H}_e + \omega_{\text{cav}} \hat{b}^\dagger \hat{b} - \sqrt{\frac{\omega_{\text{cav}}}{2}} \boldsymbol{\lambda} \cdot [\hat{\boldsymbol{\mu}} - \langle \hat{\boldsymbol{\mu}} \rangle] (\hat{b}^\dagger + \hat{b}) \\ & + \frac{1}{2} (\boldsymbol{\lambda} \cdot [\hat{\boldsymbol{\mu}} - \langle \hat{\boldsymbol{\mu}} \rangle])^2 \end{aligned} \quad (8)$$

We can see now that the mean-field energy is simply

$$E_{\text{QED-HF}} = \langle 0^e | \hat{H}_e | 0^e \rangle + \frac{1}{2} \langle 0^e | (\boldsymbol{\lambda} \cdot [\hat{\boldsymbol{\mu}}_e - \langle \hat{\boldsymbol{\mu}}_e \rangle])^2 | 0^e \rangle \quad (9)$$

because all of the terms involving the photon creation / annihilation operators vanish once we take the expectation value and integrate out the photon degrees of freedom. Note also that the dipole self-energy term, in the Born-Oppenheimer approximation, only depends on the electronic part of the dipole operator, $\hat{\boldsymbol{\mu}}_e$, because the nuclear part cancels once we take the expectation value.

From this point, one can easily adapt this polaritonic mean-field theory to obtain a QED generalization of Kohn-Sham DFT, or QED-DFT.²⁴⁻²⁶ The QED-DFT ground-state is modeled by a non-interacting state of the form given above (Eq. 3), with $|0^e\rangle$ now referring to a determinant of Kohn-Sham orbitals. The electronic part of the energy, $\langle 0^e | \hat{H}_e | 0^e \rangle$, is handled as in standard Kohn-Sham DFT, *i.e.*, it replaced by the

Kohn-Sham energy E_{KS} , which is a sum of core Hamiltonian (h) and classical Coulomb (J) contributions, plus an exchange-correlation functional of the electronic density (ρ), the gradient of the density ($\nabla\rho$), etc.:

$$E_{\text{KS}} = \sum_{\mu\nu} (h_{\mu\nu} + \frac{1}{2}J_{\mu\nu})\gamma_{\mu\nu} + f_{\text{xc}}(\rho, \nabla\rho, \dots) \quad (10)$$

with

$$J_{\mu\nu} = \sum_{\lambda\sigma} (\mu\nu|\lambda\sigma)\gamma_{\lambda\sigma} \quad (11)$$

Here, the Greek labels represent atomic basis functions, $\gamma_{\mu\nu}$ is the one-particle density matrix, and $(\mu\nu|\lambda\sigma)$ is a two-electron repulsion integral in chemists' notation.

The λ -dependent part of the energy (the dipole-self energy) is handled the same way as it is treated in QED-HF, so the total QED-DFT energy is simply

$$E_{\text{QED-DFT}} = E_{\text{KS}} + \frac{1}{2} \langle 0^e | (\boldsymbol{\lambda} \cdot [\hat{\boldsymbol{\mu}}_e - \langle \hat{\boldsymbol{\mu}}_e \rangle])^2 | 0^e \rangle \quad (12)$$

More explicitly, the dipole self-energy term can be evaluated as

$$\begin{aligned} \frac{1}{2} \langle 0^e | [\boldsymbol{\lambda} \cdot (\hat{\boldsymbol{\mu}}_e - \langle \hat{\boldsymbol{\mu}}_e \rangle)]^2 | 0^e \rangle &= \frac{1}{2} (\boldsymbol{\lambda} \cdot \langle \hat{\boldsymbol{\mu}}_e \rangle)^2 \\ &+ \sum_{\mu\nu} (\frac{1}{2}J_{\mu\nu}^{\text{DSE}} - \frac{1}{2}K_{\mu\nu}^{\text{DSE}} + O_{\mu\nu}^{\text{DSE}})\gamma_{\mu\nu} \end{aligned} \quad (13)$$

with

$$J_{\mu\nu}^{\text{DSE}} = d_{\mu\nu} \sum_{\lambda\sigma} d_{\lambda\sigma} \gamma_{\lambda\sigma} = (\boldsymbol{\lambda} \cdot \langle \hat{\boldsymbol{\mu}}_e \rangle) d_{\mu\nu} \quad (14)$$

$$K_{\mu\nu}^{\text{DSE}} = \sum_{\lambda\sigma} d_{\mu\sigma} d_{\lambda\nu} \gamma_{\lambda\sigma} \quad (15)$$

$$O_{\mu\nu}^{\text{DSE}} = -(\boldsymbol{\lambda} \cdot \langle \hat{\boldsymbol{\mu}}_e \rangle) d_{\mu\nu} - \frac{1}{2}q_{\mu\nu} \quad (16)$$

Here, $\langle \hat{\boldsymbol{\mu}}_e \rangle$ represents the expectation value of the electronic dipole operator evaluated with respect to the Kohn-Sham state, and, following Ref. 24, we have introduced

$$d_{\mu\nu} = \sum_{a \in \{x,y,z\}} \lambda_a \int \phi_{\mu}^*[-r_a] \phi_{\nu} d\tau, \quad (17)$$

and

$$q_{\mu\nu} = \sum_{ab \in \{x,y,z\}} \lambda_a \lambda_b \int \phi_{\mu}^*[-r_a r_b] \phi_{\nu} d\tau. \quad (18)$$

which are λ -weighted dipole and quadrupole integrals, respectively. The symbol ϕ_{μ} represents an atomic basis function, λ_a is a cartesian component of the coupling vector, $\boldsymbol{\lambda}$, and $r_x = x$, etc. Several terms in Eq. 13 cancel, so Eq. 12 simplifies to

$$E_{\text{QED-DFT}} = E_{\text{KS}} - \frac{1}{2} \sum_{\mu\nu} (q_{\mu\nu} + K_{\mu\nu}^{\text{DSE}})\gamma_{\mu\nu} \quad (19)$$

B. Analytic Energy Gradients for QED-DFT

When the QED-DFT problem is represented within the coherent-state basis, the gradient of the energy (Eq. 19) with respect to a perturbation, χ , is

$$\frac{\partial E_{\text{QED-DFT}}}{\partial \chi} = \frac{\partial E_{\text{KS}}}{\partial \chi} - \frac{1}{2} \frac{\partial}{\partial \chi} \sum_{\mu\nu} (q_{\mu\nu} + K_{\mu\nu}^{\text{DSE}})\gamma_{\mu\nu} \quad (20)$$

Here, $\frac{\partial E_{\text{KS}}}{\partial \chi}$ equivalent to the gradient of the energy in standard (non-QED) Kohn-Sham DFT, so we focus on the the λ -dependent term. We introduce λ -weighted derivative dipole and quadrupole integrals, defined as

$$d_{\mu\nu}^{\chi} = \frac{\partial}{\partial \chi} \sum_{a \in \{x,y,z\}} \lambda_a \int \phi_{\mu}^*[-r_a] \phi_{\nu} d\tau, \quad (21)$$

and

$$q_{\mu\nu}^{\chi} = \frac{\partial}{\partial \chi} \sum_{ab \in \{x,y,z\}} \lambda_a \lambda_b \int \phi_{\mu}^*[-r_a r_b] \phi_{\nu} d\tau. \quad (22)$$

respectively, and the final gradient expression is

$$\frac{\partial E_{\text{QED-DFT}}}{\partial \chi} = \frac{\partial E_{\text{KS}}}{\partial \chi} - \frac{1}{2} \sum_{\mu\nu} q_{\mu\nu}^{\chi} \gamma_{\mu\nu} - \sum_{\mu\nu} \gamma_{\mu\nu} \sum_{\lambda\sigma} \gamma_{\lambda\sigma} d_{\mu\sigma}^{\chi} d_{\lambda\nu} \quad (23)$$

III. COMPUTATIONAL DETAILS

We have implemented the QED-DFT approach, together with QED-DFT analytic energy gradients in `hilbert`,⁵⁶ which is a plugin to the `PSI4`⁵⁷ electronic structure package. All cavity-free DFT calculations were performed using the aug-cc-pVDZ basis set and the dispersion-corrected B3LYP-D3BJ functional. QED-DFT calculations initially use the STO-3G basis-set to obtain an initial guess for the reoriented / relaxed molecular geometry; final geometries were refined using the same basis set and functional from the cavity-free DFT calculations. Following Ref. 42, all calculations use a cavity frequency (ω_{cav}) and coupling strength (λ) equal to 1.5 eV and 0.1 a.u., respectively.

Optimal geometries for the reactant (educt) and product species relevant to the Diels-Alder reactions we consider were performed using the `Pysisyphus`⁵⁸ software suite, which we interfaced with `hilbert` to provide access to QED-DFT gradients. The calculations of cavity-free and cavity-embedded species were performed using DFT and QED-DFT, respectively. Initial estimates of transition state geometries were determined from the nudged elastic band (NEB) method⁵⁹⁻⁶¹ and further refined using the improved dimer method⁶² within `Pysisyphus`.

The QED-DFT energy depends on the relative orientation of the molecular species and the cavity-mode polarization axis. For this reason, a traditional internal coordinate system is a poor choice in that it overlooks both the spatial orientation

and the system’s center of mass; procedures for transitioning back to cartesian coordinates can be ambiguous. As such, all geometry optimizations in this work were performed using translation-rotation internal coordinates⁶³ (TRIC), which account for the energy contributions from rotations. Pysisyphus supports the TRIC system.

IV. RESULTS AND DISCUSSION

In gas- or solution-phase small-molecule reactions, it is reasonable to expect that the molecular species are free to rotate with respect to a fixed coordinate frame. Without an explicit mechanism to fix the molecular orientation with respect to the cavity-mode polarization, it is important to understand the rotational energy landscape and its impact on the optimal reaction pathway and any inferred properties. We emphasize this importance by revisiting the study from Ref. 42 that explored the thermodynamics of a Diels-Alder cycloaddition involving cyclopentadiene and acrylonitrile in an optical cavity.

A. Rotational energy landscape

Figure 2 illustrates the energy of the *endo* Diels-Alder product of cyclopentadiene and acrylonitrile (see Fig. 1) as a function of the relative orientation of the molecular dipole moment and the cavity mode polarization axis, which is aligned along the z -direction. In this example, the internal coordinates of the molecule are frozen at the optimal values from a geometry optimization performed in the absence of the cavity.

The surface on the left-hand side of Fig. 2 represents the energy of the system as a function of the direction of the total dipole moment, which is characterized by the inclination (ϕ) and azimuthal (θ) angles relative to the cavity mode polarization axis (the z -axis.) The radius of the surface (ρ) is proportional to the difference between the energy at ϕ and θ and the energy at the minimum energy orientation (MEO) at $\phi = \phi'$ and $\theta = \theta'$, *i.e.*,

$$\rho(\phi, \theta) = E(\phi, \theta | \mathbf{R}) - E(\phi', \theta' | \mathbf{R}) + \rho_0 \quad (24)$$

where \mathbf{R} represents the fixed internal coordinates of the cavity-free *endo* Diels-Alder product. The radial function is given an arbitrary minimum length ($\rho_0 = 0.10 \text{ kcal mol}^{-1}$) so that energy changes appear as deformations to a small sphere. The color of the surface also reflects the difference in energies evaluated at a given orientation and at the MEO. The color gradient is defined on the right-hand side of the figure, where the energy landscape is also presented as a heat map.

The MEO corresponds to $\phi' = -44.0^\circ$ and $\theta' = 75.1^\circ$, where the molecular dipole is oriented along the xy -plane. The energy increases rapidly as the dipole orientation approaches the z -axis ($\phi \rightarrow 0^\circ$ or 180°) for any value of θ . To understand this behavior, consider the form of the QED-DFT energy, when the Hamiltonian is represented within the coherent-state basis. Equation 12 suggests that the system will be most stable when the molecule is oriented such that the dipole self-energy

is minimized. If the cavity mode is polarized along the z direction [*i.e.*, $\lambda = (0, 0, \lambda)$], the dipole self-energy, E_{DSE} , is

$$\begin{aligned} E_{\text{DSE}} &= \frac{1}{2} \langle 0^e | (\lambda \cdot [\hat{\mu} - \langle \hat{\mu} \rangle])^2 | 0^e \rangle \\ &= \frac{1}{2} \lambda^2 \langle 0^e | (\hat{\mu}_e^z - \langle \hat{\mu}_e^z \rangle)^2 | 0^e \rangle \end{aligned} \quad (25)$$

Hence, the key quantity for understanding the rotational energy landscape of the cavity-bound species is the variance in the dipole moment along the z direction. Indeed, the dipole variance along z is minimized at the MEO, and maximized when $\phi = -5.8^\circ$ and $\theta = -18.9^\circ$ at the highest energy orientation (HEO) of the molecule.

The HEO lies 14.5 kcal/mol higher in energy than the MEO. This gap is substantial and is greater in magnitude to the cavity-free activation energy for the Diels-Alder reaction that produces this product (13.5 kcal/mol). These results have significant implications for the thermodynamics and kinetics of chemical reactions carried out in optical cavities. In the absence of a mechanism to restrict the rotational degrees of freedom, a cavity-embedded molecule should reorient to minimize the dipole self-energy. Conclusions derived from energetic analyses carried out at fixed molecular orientations miss this important detail.

B. Challenges when optimizing non-bonded complexes

As mentioned in Sec. III, *ab initio* QED geometry optimizations should be performed using a coordinate system that captures the orientation dependence of the energy; we use the TRIC system. This choice alone does not completely eliminate the numerical difficulties in optimizing geometries of cavity-embedded species, particularly for non-bonded complexes. For example, in the Diels-Alder educt structure, acrylonitrile has a larger dipole variance than cyclopentadiene, so the former fragment may experience larger forces due to the dipole self-energy contribution to the gradient. As a result, situations arise where the system moves away from the desired geometry in the course of an optimization. Figure 3 illustrates the educt structures for the *endo* and *exo* pathways (left and right panels, respectively) that were optimized with the system interacting with a cavity mode polarized along different cartesian axes. The axes are chosen to be the same as those in Ref. 42, where the x -axis is along the forming carbon-carbon bond, and the yz plane is along the plane of the cyclopentadiene such that the xy -plane intersects its sp^3 hybridized carbon and the xz plane intersects the adjacent carbons. For these illustrative calculations, we used a minimal (STO-3G) basis set, and the cavity coupling strength, λ , was 0.1 a.u. Panels (a) and (e) show the structures in the absence of the cavity, which were taken from Ref. 42 (and optimized at the MP2/cc-pVDZ level of theory). In the other panels, we observe cases where the optimization leads to stationary points that are not relevant for the cyclization reaction in question. Depending on the cavity mode polarization, the fragments may align side by side [panels (c), (g), and (h)] or the plane of the acrylonitrile can rotate so that it is no longer parallel to the plane of

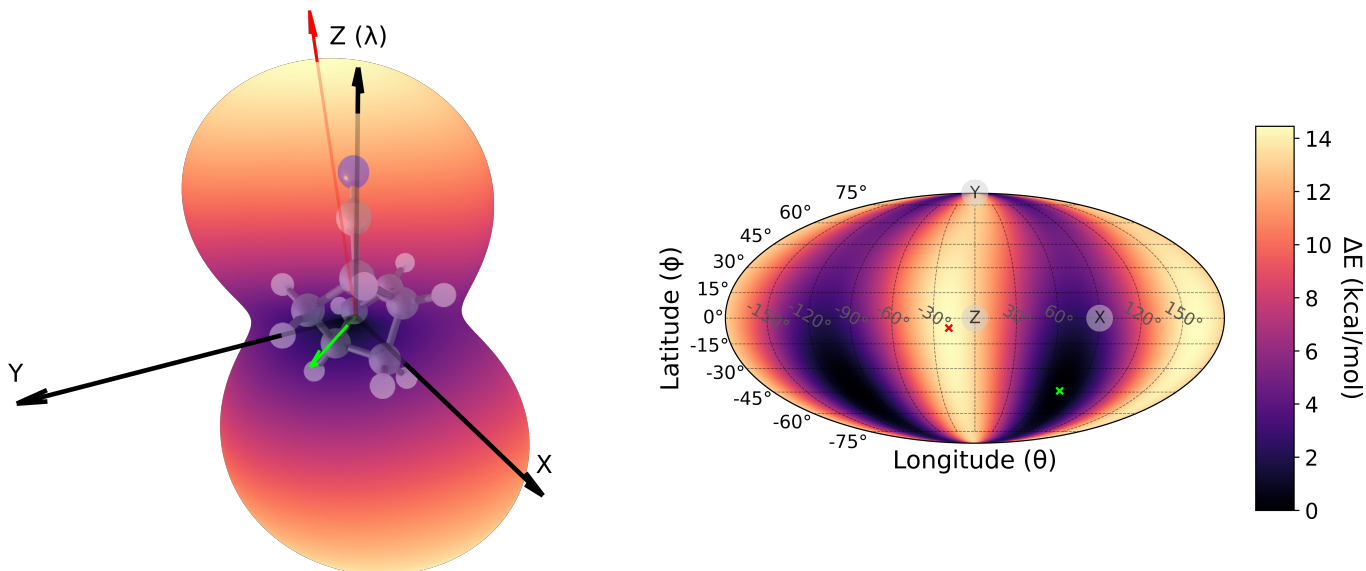


FIG. 2. The energy profile of the *endo* Diels-Alder product of cyclopentadiene and acrylonitrile as a function of the spatial orientation of the molecular dipole moment for the cavity-free geometry with respect to a *z*-polarized cavity. The *endo* product is visualized in (a), with the dipole oriented along the *z*-axis. The energy profile is represented in two ways: (a) as a deformed sphere where the radius and color at each point represent the relative energy difference from the minimum energy orientation, and (b) as a Mollweide projection where the energy gap (color), latitude, and longitude coordinates are related to the spherical coordinates ρ , ϕ , and θ , respectively. The minimum energy orientation (MEO) and highest energy orientation (HEO) are denoted by green and red arrows and crosses, respectively.

the cyclopentadiene [panel (d)].

The lowest energy educt configurations for the *endo* and *exo* pathways are associated with structures optimized starting from the *x*-polarized cavity mode [panels (b) and (f), respectively]; notably, these are the structures that most closely resemble the relevant educt geometries for the cavity-free Diels-Alder cycloaddition reaction. Structures optimized starting from the *y*-polarized cavity mode [panels (c) and (g)] are not too much higher in energy [0.1 and 0.2 kcal mol⁻¹, relative to the structures in panels (b) and (f), respectively]. On the other hand, optimized structures starting from the *z*-polarized cavity mode [panels (d) and (h)] lie a bit higher in energy [5.0 and 1.0 kcal mol⁻¹, relative to the structures in panels (b) and (e), respectively].

The large variations in optimized structures depicted in Fig. 3, some of which are qualitatively different than the educt structures relevant to the cyclization reaction, are problematic and motivate the need for a robust protocol for geometry optimizations in the presence of an optical cavity. As such, we have developed and applied the following procedure. An initial constrained optimization is performed such that the entire complex can rotate into its optimal orientation relative to the cavity mode polarization axis. For the educt structures relevant to the Diels-Alder reactions considered in this work, the relative orientations of the fragments are partially fixed by constraining the distance between the bond-forming carbon atoms, as well as the dihedral angles between fragment planes. Once the optimal orientation of the constrained educt structure has been identified, a full geometry optimization can be performed. With this procedure, the fully optimized educt structures associated with the *endo* path differ in energy by

only ≈ 0.01 kcal mol⁻¹, while those for the *exo* path differ by ≈ 0.03 – 0.04 kcal mol⁻¹, regardless of the initial relative orientation of the complex and the cavity mode polarization axis. While we have focused this discussion on the optimization of non-bonded educt reactant structures, we note that this optimization procedure provides similarly robust results for the *endo/exo* product structures; when starting from different orientations relative to the cavity mode polarization axis, the resulting structures differ in energy by at most 0.03 kcal mol⁻¹.

C. Enthalpies and barrier heights the Diels-Alder reaction

We now turn our attention to the the cavity-induced changes to the thermodynamics of the Diels-Alder reactions depicted in Fig. 1. For calculations on relaxed structures that account for cavity interactions, *endo/exo* reactant and product geometries are identified initially within a minimal basis, using the procedure outlined in Sec. IV B. These initial structures are further refined using the aug-cc-pVDZ basis set. Given optimized educt and product geometries, we locate transition states using the NEB implementation in Pysisyphus, which can capture the cavity-induced rotation of the molecule as the cycloaddition progresses. This rotation is necessary to account for the different orientation preferences of the optimized educt and product structures. The transition state structures are further refined using the improved dimer method⁶² within Pysisyphus.

Table I contains reaction enthalpies (H), forward activation energies (E_a^f), and backward activation energies (E_a^b) for the *endo* and *exo* pathways of the Diels-Alder reaction in the ab-

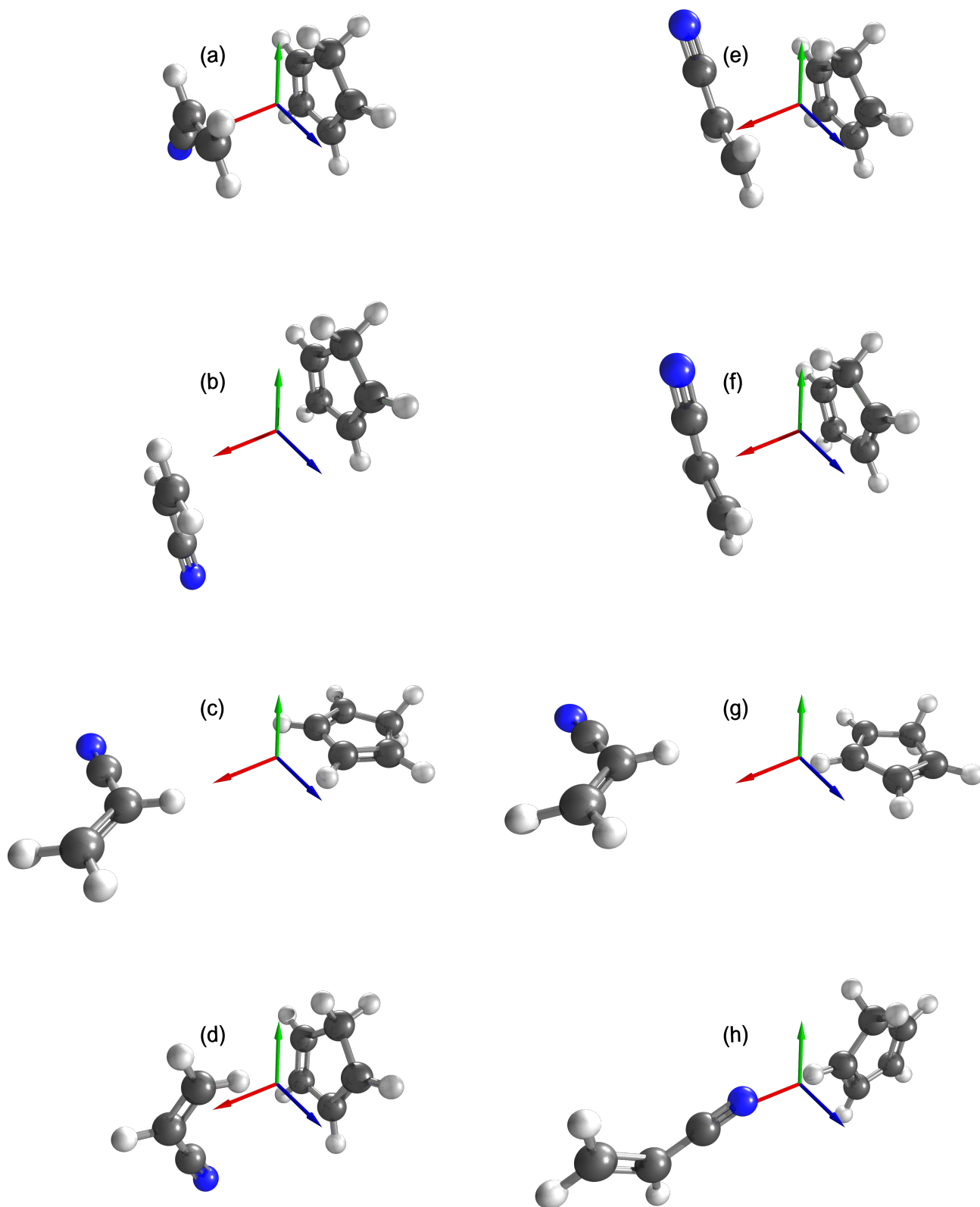


FIG. 3. Educt structures for the *endo/exo* pathways optimized under different cavity mode polarizations. The left (a)-(d) and right (e)-(h) columns correspond to the *endo* and *exo* geometries. The rows correspond to the reference geometry (a), (e), the converged geometries for the initial *x*-, *y*-, and *z*- polarizations [panels (b),(f); (c),(g); (d),(h), respectively].

path	structures	H	E_a^f	E_a^b
$\lambda = 0.0$				
<i>endo</i>	—	-22.6	13.5	36.1
<i>exo</i>	—	-22.3	13.7	35.9
$\lambda = 0.1$				
<i>endo</i>	optimized	-9.4	34.6	44.0
	fixed (x)	-10.3	34.1	44.4
	fixed (y)	-32.4	12.7	45.1
	fixed (z)	-28.3	14.3	42.6
<i>exo</i>	optimized	-11.7	30.8	42.6
	fixed (x)	-9.9	33.2	43.2
	fixed (y)	-32.4	14.2	46.6
	fixed (z)	-27.8	15.7	43.5

TABLE I. Reaction enthalpies and forward/backward activation energies (kcal mol⁻¹) for the *endo* and *exo* pathways for the different structures and cavity mode polarizations.

sence of the cavity ($\lambda = 0.0$ a.u.) and at $\lambda = 0.1$ a.u. For the cavity-free case, the structures were optimized at the B3LYP-D3BJ/aug-cc-pVDZ level of theory. We consider four sets of calculations on cavity-embedded species, one set where the structures are fully optimized at the QED-B3LYP-D3BJ/aug-cc-pVDZ level of theory, and three sets where we use fixed structures optimized in the absence of the cavity and fixed orientations relative to different cavity mode polarization axes.

In the cavity-free case, the *endo* pathway is slightly favored both thermodynamically and kinetically, by less than 1 kcal mol⁻¹. The question so-often posed in *ab initio* cavity QED studies is then, can ultra-strong light-matter coupling induce meaningful changes to the enthalpy or barrier height for these reactions? The answer to this question is, of course, yes, but wildly different conclusions can be drawn depending on whether the structures are relaxed in the presence of the cavity or, with fixed structures, how the molecule is oriented with respect to the cavity mode polarization axis. Focusing on the fully optimized structures first, we observe the following: First, the enthalpy of the reaction is reduced in magnitude by a factor of two, for both pathways. Second, the thermodynamic favorability of the reaction is reversed, with the enthalpy for the *exo* path being about 2 kcal mol⁻¹ more negative than that for the *endo* path. Third, the barrier to the forward reaction increases by more than a factor of two for both paths, with the barrier height being higher in the case of the *endo* path by nearly 4 kcal mol⁻¹. These results suggest that ultrastrong light-matter coupling could be used to slightly alter the preferred cycloaddition product, with the caveat that the forward reaction would be much less favorable for the cavity embedded system, relative to the original cavity-free system.

The story is quite different when considering unrelaxed geometries with fixed orientations relative to the cavity mode polarization axis. For both the *endo* and *exo* pathways, we find that an *x*-polarized cavity mode leads to similar results as with fully relaxed structures; the magnitudes of the enthalpies are

reduced by more than a factor of two, and the barrier heights more than double. On the other hand, *y*- and *z*-polarized cavity modes lead to significantly more negative enthalpies, while changing the forward reaction barrier heights by only 1–2 kcal mol⁻¹. For all polarizations, the *endo* product is thermodynamically preferred, but never by more than 0.6 kcal mol⁻¹. We stress that this is the opposite result obtained from calculations on fully-optimized structures, which predict that the *exo* product is thermodynamically preferred by 2.3 kcal mol⁻¹.

V. CONCLUSIONS

A number of recent theoretical studies have focused on the application of *ab initio* cavity QED methodologies to the ground-state electronic structure of cavity embedded species, in an effort to identify cases where ultra-strong light-matter coupling leads to useful or interesting changes to chemistry. The common theme in these studies is that non-trivial changes (*e.g.*, to reaction enthalpies, barrier heights, etc.) can be realized, given large enough light-matter coupling strengths, but these changes tend to display a pronounced orientational dependence. None of the studies cited in Sec. I consider geometry relaxation or rotational effects that should be induced by the very large coupling strengths employed in those works.

In this study, we have shown that geometry relaxation effects can lead one to draw qualitatively different conclusions regarding the impact of an optical cavity on ground-state chemistry, as compared to calculations involving fixed structures and orientations relative to the cavity mode axis. We have demonstrated this point by revisiting the Diels-Alder cycloaddition reactions considered in Ref. 42. Without a physical mechanism to constrain the orientation of the molecule in the cavity, the reactant / transition state / product species reorient in a way that eliminates the dependence on the initial relative orientations of the molecular components and the cavity mode polarization axis. Our calculations involving fully-relaxed structures suggest that the *exo* cycloaddition product is the thermodynamically favored one at large coupling strengths, while calculations on fixed structures lead to the opposite interpretation, regardless of the chosen polarization axis. As such, conclusions drawn from energetic analyses based on *ab initio* QED calculations that use fixed molecular structures should be viewed with caution.

Supporting Information Relaxed and unrelaxed geometries for the *endo* and *exo* Diel-Alder reactions within a *z*-polarized cavity at the B3LYP-D3BJ/aug-cc-pVDZ level of theory.

ACKNOWLEDGMENTS

This material is based upon work supported by the National Science Foundation under Grant No. CHE-2100984.

DATA AVAILABILITY

The data that support the findings of this study are available from the corresponding author upon reasonable request.

- ¹D. G. Lidzey, D. D. C. Bradley, M. S. Skolnick, T. Virgili, S. Walker, and D. M. Whittaker, “Strong exciton–photon coupling in an organic semiconductor microcavity,” *Nature* **395**, 53–55 (1998).
- ²J. Bellessa, C. Bonnard, J. C. Plenet, and J. Mugnier, “Strong coupling between surface plasmons and excitons in an organic semiconductor,” *Phys. Rev. Lett.* **93**, 036404 (2004).
- ³E. Orgiu, J. George, J. A. Hutchison, E. Devaux, J. F. Dayen, B. Doudin, F. Stellacci, C. Genet, J. Schachenmayer, C. Genes, G. Pupillo, P. Samorì, and T. W. Ebbesen, “Conductivity in organic semiconductors hybridized with the vacuum field,” *Nat. Mater.* **14**, 1123–1129 (2015).
- ⁴T. W. Ebbesen, “Hybrid light–matter states in a molecular and material science perspective,” *Acc. Chem. Res.* **49**, 2403–2412 (2016).
- ⁵K. Chevrier, J. M. Benoit, C. Symonds, S. K. Saikin, J. Yuen-Zhou, and J. Bellessa, “Anisotropy and controllable band structure in suprawavelength polaritonic metasurfaces,” *Phys. Rev. Lett.* **122**, 173902 (2019).
- ⁶J. A. Hutchison, T. Schwartz, C. Genet, E. Devaux, and T. W. Ebbesen, “Modifying chemical landscapes by coupling to vacuum fields,” *Angew. Chem. Int. Ed.* **51**, 1592–1596 (2012).
- ⁷A. Thomas, J. George, A. Shalabney, M. Dryzhakov, S. J. Varma, J. Moran, T. Chervy, X. Zhong, E. Devaux, C. Genet, J. A. Hutchison, and T. W. Ebbesen, “Ground-state chemical reactivity under vibrational coupling to the vacuum electromagnetic field,” *Angew. Chem. Int. Ed.* **55**, 11462–11466 (2016).
- ⁸A. Thomas, L. Lethuillier-Karl, K. Nagarajan, R. M. Vergauwe, J. George, T. Chervy, A. Shalabney, E. Devaux, C. Genet, J. Moran, *et al.*, “Tilting a ground-state reactivity landscape by vibrational strong coupling,” *Science* **363**, 615–619 (2019).
- ⁹K. Stranius, M. Hertzog, and K. Börjesson, “Selective manipulation of electronically excited states through strong light–matter interactions,” *Nature Communications* **9**, 2273 (2018).
- ¹⁰J. Lather, P. Bhatt, A. Thomas, T. W. Ebbesen, and J. George, “Cavity catalysis by cooperative vibrational strong coupling of reactant and solvent molecules,” *Angew. Chem. Int. Ed.* **58**, 10635–10638 (2019).
- ¹¹A. D. Dunkelberger, B. S. Simpkins, I. Vurgaftman, and J. C. Owrutsky, “Vibration-cavity polariton chemistry and dynamics,” *Annual Review of Physical Chemistry* **73**, 429–451 (2022).
- ¹²R. F. Ribeiro, L. A. Martínez-Martínez, M. Du, J. Campos-Gonzalez-Angulo, and J. Yuen-Zhou, “Polariton chemistry: controlling molecular dynamics with optical cavities,” *Chem. Sci.* **9**, 6325–6339 (2018).
- ¹³I. Foley, Jonathan J., J. F. McTague, and I. DePrince, A. Eugene, “Ab initio methods for polariton chemistry,” *Chemical Physics Reviews* **4**, 041301 (2023), https://pubs.aip.org/aip/cpr/article-pdf/doi/10.1063/5.0167243/18165450/041301_1_5.0167243.pdf.
- ¹⁴M. Ruggenthaler, F. Mackenroth, and D. Bauer, “Time-dependent Kohn-Sham approach to quantum electrodynamics,” *Phys. Rev. A* **84**, 042107 (2011).
- ¹⁵I. V. Tokatly, “Time-dependent density functional theory for many-electron systems interacting with cavity photons,” *Phys. Rev. Lett.* **110**, 233001 (2013).
- ¹⁶M. Ruggenthaler, J. Flick, C. Pellegrini, H. Appel, I. V. Tokatly, and A. Rubio, “Quantum-electrodynamical density-functional theory: Bridging quantum optics and electronic-structure theory,” *Phys. Rev. A* **90**, 012508 (2014).
- ¹⁷C. Pellegrini, J. Flick, I. V. Tokatly, H. Appel, and A. Rubio, “Optimized effective potential for quantum electrodynamical time-dependent density functional theory,” *Phys. Rev. Lett.* **115**, 093001 (2015).
- ¹⁸J. Flick, C. Schäfer, M. Ruggenthaler, H. Appel, and A. Rubio, “Ab initio optimized effective potentials for real molecules in optical cavities: Photon contributions to the molecular ground state,” *ACS Photonics* **5**, 992–1005 (2018).
- ¹⁹R. Jestädt, M. Ruggenthaler, M. J. T. Oliveira, A. Rubio, and H. Appel, “Light–matter interactions within the Ehrenfest–Maxwell–Pauli–Kohn–Sham framework: fundamentals, implementation, and nano-optical applications,” *Adv. Phys.* **68**, 225–333 (2019).
- ²⁰J. Flick, D. M. Welakuh, M. Ruggenthaler, H. Appel, and A. Rubio, “Light–matter response in nonrelativistic quantum electrodynamics,” *ACS Photonics* **6**, 2757–2778 (2019).
- ²¹J. Flick and P. Narang, “Ab initio polaritonic potential-energy surfaces for excited-state nanophotonics and polaritonic chemistry,” *J. Chem. Phys.* **153**, 094116 (2020).
- ²²C. Schäfer, J. Flick, E. Ronca, P. Narang, and A. Rubio, “Shining light on the microscopic resonant mechanism responsible for cavity-mediated chemical reactivity,” *Nature Communications* **13**, 7817 (2022).
- ²³M. Ruggenthaler, D. Sidler, and A. Rubio, “Understanding polaritonic chemistry from ab initio quantum electrodynamics,” *Chemical Reviews* **123**, 11191–11229 (2023).
- ²⁴N. Vu, G. M. McLeod, K. Hanson, and A. E. I. DePrince, “Enhanced diastereocontrol via strong light–matter interactions in an optical cavity,” *The Journal of Physical Chemistry A* **126**, 9303–9312 (2022).
- ²⁵F. Pavošević and A. Rubio, “Wavefunction embedding for molecular polaritons,” *J. Chem. Phys.* **157**, 094101 (2022).
- ²⁶M. D. Liebenthal, N. Vu, and A. E. I. DePrince, “Assessing the effects of orbital relaxation and the coherent-state transformation in quantum electrodynamics density functional and coupled-cluster theories,” *The Journal of Physical Chemistry A* **127**, 5264–5275 (2023).
- ²⁷J. Yang, Q. Ou, Z. Pei, H. Wang, B. Weng, Z. Shuai, K. Mullen, and Y. Shao, “Quantum-electrodynamical time-dependent density functional theory within Gaussian atomic basis,” *J. Chem. Phys.* **155**, 064107 (2021).
- ²⁸J. Yang, Z. Pei, E. C. Leon, C. Wickizer, B. Weng, Y. Mao, Q. Ou, and Y. Shao, “Cavity quantum-electrodynamical time-dependent density functional theory within Gaussian atomic basis. II. Analytic energy gradient,” *J. Chem. Phys.* **156**, 124104 (2022).
- ²⁹T. S. Haugland, C. Schäfer, E. Ronca, A. Rubio, and H. Koch, “Intermolecular interactions in optical cavities: An ab initio qed study,” *J. Chem. Phys.* **154**, 094113 (2021).
- ³⁰J. McTague and J. J. Foley, “Non-hermitian cavity quantum electrodynamics–configuration interaction singles approach for polaritonic structure with ab initio molecular hamiltonians,” *J. Chem. Phys.* **156**, 154103 (2022).
- ³¹N. Vu, D. Mejia-Rodriguez, N. P. Bauman, A. Panyala, E. Mutlu, N. Govind, and J. J. I. Foley, “Cavity quantum electrodynamics complete active space configuration interaction theory,” *Journal of Chemical Theory and Computation* **20**, 1214–1227 (2024), <https://doi.org/10.1021/acs.jctc.3c01207>.
- ³²J. D. Weidman, M. S. Dadgar, Z. J. Stewart, B. G. Peyton, I. S. Ulusoy, and A. K. Wilson, “Cavity-modified molecular dipole switching dynamics,” *The Journal of Chemical Physics* **160**, 094111 (2024), https://pubs.aip.org/aip/jcp/article-pdf/doi/10.1063/5.0188471/19708269/094111_1_5.0188471.pdf.
- ³³T. S. Haugland, E. Ronca, E. F. Kjønstad, A. Rubio, and H. Koch, “Coupled cluster theory for molecular polaritons: Changing ground and excited states,” *Phys. Rev. X* **10**, 041043 (2020).
- ³⁴U. Mordovina, C. Bungey, H. Appel, P. J. Knowles, A. Rubio, and F. R. Manby, “Polaritonic coupled-cluster theory,” *Phys. Rev. Res.* **2**, 023262 (2020).
- ³⁵J. Fregoni, T. S. Haugland, S. Pipolo, T. Giovannini, H. Koch, and S. Corni, “Strong coupling between localized surface plasmons and molecules by coupled cluster theory,” *Nano Lett.* **21**, 6664–6670 (2021).
- ³⁶A. E. DePrince, “Cavity-modulated ionization potentials and electron affinities from quantum electrodynamics coupled-cluster theory,” *J. Chem. Phys.* **154**, 094112 (2021).
- ³⁷F. Pavošević and J. Flick, “Polaritonic unitary coupled cluster for quantum computations,” *J. Phys. Chem. Lett.* **12**, 9100–9107 (2021).
- ³⁸R. R. Riso, T. S. Haugland, E. Ronca, and H. Koch, “On the characteristic features of ionization in qed environments,” *J. Chem. Phys.* **156**, 234103 (2022).
- ³⁹F. Pavošević, S. Hammes-Schiffer, A. Rubio, and J. Flick, “Cavity-modulated proton transfer reactions,” *Journal of the American Chemical Society* **144**, 4995–5002 (2022).
- ⁴⁰M. L. Vidal, F. R. Manby, and P. J. Knowles, “Polaritonic effects in the vibronic spectrum of molecules in an optical cavity,” *J. Chem. Phys.* **156**, 204119 (2022).
- ⁴¹M. D. Liebenthal, N. Vu, and A. E. DePrince III, “Equation-of-motion cavity quantum electrodynamics coupled-cluster theory for electron attachment,” *J. Chem. Phys.* **156**, 054105 (2022).
- ⁴²F. Pavošević, R. L. Smith, and A. Rubio, “Computational study on the cat-

- alytic control of endo/exo diels-alder reactions by cavity quantum vacuum fluctuations,” *Nature Communications* **14**, 2766 (2023).
- ⁴³F. Pavošević, R. L. Smith, and A. Rubio, “Cavity click chemistry: Cavity-catalyzed azide–alkyne cycloaddition,” *The Journal of Physical Chemistry A* **127**, 10184–10188 (2023).
- ⁴⁴M. Romanelli, R. R. Riso, T. S. Haugland, E. Ronca, S. Corni, and H. Koch, “Effective single-mode methodology for strongly coupled multimode molecular-plasmon nanosystems,” *Nano Letters* **23**, 4938–4946 (2023).
- ⁴⁵J. P. Philbin, T. S. Haugland, T. K. Ghosh, E. Ronca, M. Chen, P. Narang, and H. Koch, “Molecular van der waals fluids in cavity quantum electrodynamics,” *The Journal of Physical Chemistry Letters* **14**, 8988–8993 (2023).
- ⁴⁶R. R. Riso, L. Grazioli, E. Ronca, T. Giovannini, and H. Koch, “Strong coupling in chiral cavities: Nonperturbative framework for enantiomer discrimination,” *Phys. Rev. X* **13**, 031002 (2023).
- ⁴⁷J. D. Mallory and A. E. DePrince, “Reduced-density-matrix-based ab initio cavity quantum electrodynamics,” *Phys. Rev. A* **106**, 053710 (2022).
- ⁴⁸M. Bauer and A. Dreuw, “Perturbation theoretical approaches to strong light–matter coupling in ground and excited electronic states for the description of molecular polaritons,” *J. Chem. Phys.* **158**, 124128 (2023).
- ⁴⁹T. S. Haugland, J. P. Philbin, T. K. Ghosh, M. Chen, H. Koch, and P. Narang, “Understanding the polaritonic ground state in cavity quantum electrodynamics,” arXiv preprint, arXiv:2307.14822 (2023).
- ⁵⁰S. Ayad, V. Posey, A. Das, J. M. Montgomery, and K. Hanson, “Enantioenrichment of racemic binol by way of excited state proton transfer,” *Chem. Commun.* **55**, 1263–1266 (2019).
- ⁵¹M. Severi and F. Zerbetto, “Polaritonic chemistry: Hindering and easing ground state polyenic isomerization via breakdown of $\sigma\pi$ separation,” *The Journal of Physical Chemistry Letters* **14**, 9145–9149 (2023).
- ⁵²H. Spohn, *Dynamics of Charged Particles and their Radiation Field* (Cambridge Univ. Press, Cambridge, 2004).
- ⁵³M. Ruggenthaler, N. Tancogne-Dejean, J. Flick, H. Appel, and A. Rubio, “From a quantum-electrodynamical light–matter description to novel spectroscopies,” *Nat. Rev. Chem.* **2**, 0118 (2018).
- ⁵⁴A. Mandal, T. D. Krauss, and P. Huo, “Polariton-mediated electron transfer via cavity quantum electrodynamics,” *J. Phys. Chem. B* **124**, 6321–6340 (2020).
- ⁵⁵P. Hohenberg and W. Kohn, “Inhomogeneous electron gas,” *Phys. Rev.* **136**, B864–B871 (1964).
- ⁵⁶A. E. DePrince III, “Hilbert: a space for quantum chemistry plugins to Psi4,” (2020), <https://github.com/edeprince3/hilbert> (last accessed July, 2023).
- ⁵⁷D. G. A. Smith, L. A. Burns, A. C. Simmonett, R. M. Parrish, M. C. Schieber, R. Galvelis, P. Kraus, H. Kruse, R. Di Remigio, A. Alenaizan, A. M. James, S. Lehtola, J. P. Misiewicz, M. Scheurer, R. A. Shaw, J. B. Schriber, Y. Xie, Z. L. Glick, D. A. Sirianni, J. S. O’Brien, J. M. Wal-drop, A. Kumar, E. G. Hohenstein, B. P. Pritchard, B. R. Brooks, H. F. Schaefer, A. Y. Sokolov, K. Patkowski, A. E. DePrince, U. Bozkaya, R. A. King, F. A. Evangelista, J. M. Turney, T. D. Crawford, and C. D. Sherrill, “Psi4 1.4: Open-source software for high-throughput quantum chemistry,” *J. Chem. Phys.* **152**, 184108 (2020).
- ⁵⁸J. Steinmetzer, S. Kupfer, and S. Gräfe, “pysisyphus: Exploring potential energy surfaces in ground and excited states,” *International Journal of Quantum Chemistry* **121**, e26390 (2021).
- ⁵⁹B. Peters, A. Heyden, A. T. Bell, and A. Chakraborty, “A growing string method for determining transition states: Comparison to the nudged elastic band and string methods,” *The Journal of Chemical Physics* **120**, 7877–7886 (2004).
- ⁶⁰P. M. Zimmerman, “Growing string method with interpolation and optimization in internal coordinates: Method and examples,” *The Journal of Chemical Physics* **138**, 184102 (2013).
- ⁶¹J. Zhang, H. Zhang, H. Ye, and Y. Zheng, “Free-end adaptive nudged elastic band method for locating transition states in minimum energy path calculation,” *The Journal of Chemical Physics* **145**, 094104 (2016).
- ⁶²A. Heyden, A. T. Bell, and F. J. Keil, “Efficient methods for finding transition states in chemical reactions: Comparison of improved dimer method and partitioned rational function optimization method,” *The Journal of Chemical Physics* **123**, 224101 (2005).
- ⁶³L.-P. Wang and C. Song, “Geometry optimization made simple with translation and rotation coordinates,” *The Journal of Chemical Physics* **144**, 214108 (2016).